eJSSNT Regular Paper

e-Journal of Surface Science and Nanotechnology **24**, 21–25 (2026)

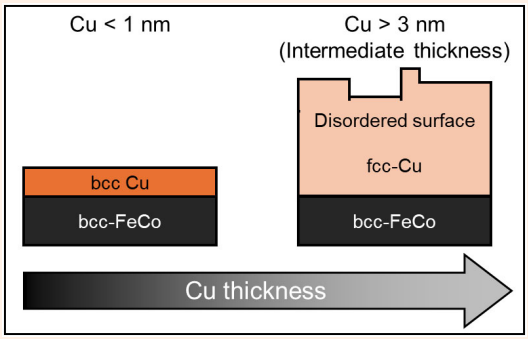
Initial Growth Process of Cu Thin Films on bcc-FeCo/MgO(100) via Molecular Beam Epitaxy

Shingo Takezawa,[a, b] Michele Riva,[c] Florian Dörr,[c] Micheal Schmid,[c] Taisuke Sasaki,[b] Takanobu Hiroto,[b] Masato Kotsugi,[a] Koichiro Yaji,[b, d] Yuya Sakuraba,[b] Naoka Nagamura [a, b, e, †]

[a] *Department of Materials Science and Technology, Tokyo University of Science, Katsushika-ku, Tokyo 125-8585, Japan*
[b] *National Institute for Materials Science, Tsukuba, Ibaraki 305-0047, Japan*
[c] *Institute of Applied Physics, TU Wien, Wiedner Hauptstraße, Vienna 1040, Austria*
[d] *Unprecedented-scale Data Analytics Center, Tohoku University, Sendai, Miyagi 980-8577, Japan*
[e] *Research Institute of Electrical Communication, Tohoku University, Sendai, Miyagi 980-8577, Japan*
[†] *Corresponding author: NAGAMURA.Naoka@nims.go.jp*

Received: 10 October, 2025; Accepted: 1 February, 2026; J-STAGE Advance Publication: 26 February, 2026; Published: 26 February, 2026

We investigated the thickness-dependent structural evolution of Cu/FeCo(100) thin films grown by molecular beam epitaxy (MBE). At the initial stage of growth, Cu adopted a body-centered cubic (bcc) structure templated by the underlying FeCo substrate. Once the Cu thickness exceeded approximately 3 nm, a structural transformation into the face-centered cubic (fcc) phase was observed. The MBE-grown films exhibited interfacial dislocations and developed a disordered surface in the thickness range of 3–5 nm. Although metastable ultrathin bcc-Cu films on FeCo(100) grown by MBE are less stable than sputtered multilayers, MBE offers a unique advantage: it enables *in-situ* advanced characterization such as angle-resolved photoemission spectroscopy (ARPES) in the ultrathin regime around 1 nm. This capability is essential for designing high-performance devices and probing interface-driven electronic phenomena.



Keywords *Thin film; Copper; Nanostructures; Molecular beam epitaxy*

I. INTRODUCTION

The growth process of thin films is an important topic in surface science, as it is strongly influenced by interactions at the film/substrate interface [1]. Bulk copper typically crystallizes in a face-centered cubic (fcc) structure, but it can adopt a body-centered cubic (bcc) structure when templated by an appropriate substrate. However, such bcc-Cu films often contain numerous defects, steps, and disordered regions [2–4]. Recently, single-phase, low-defect bcc-Cu thin films have been reported in sputtered FeCo/Cu/FeCo(100) multilayers [5–8]. These multilayers exhibit a high magnetoresistance ratio (40.5 %) when used as trilayer current-in-plane giant magnetoresistance (GMR) devices [5], underscoring their potential for spintronic applications. The exceptionally high GMR performance has been attributed to the formation of continuous Cu/FeCo(100) interfaces, directly linking the crystallography of the Cu layer to device functionality. Sputtered bcc-Cu films on TiN(100) have been reported to undergo a structural transformation into the fcc phase once the Cu thickness exceeds approximately 4–5 nm [9]. These findings highlight the importance of a systematic study for the thickness-dependent structural changes in Cu/FeCo(100) at the initial stages of growth, especially in view of potential future applications.

As noted above, many previous studies on thin film heterostructures have employed sputter deposition, owing to strong film adhesion and applicability to a wide range of materials. In contrast, molecular beam epitaxy (MBE) provides advantages as it enables precise control of film thickness in the atomic level in ultra-high vacuum (UHV) conditions. Moreover, establishing a reliable MBE growth process makes it possible to prepare atomically clean surfaces and to employ advanced *in-situ* characterization techniques owing to the portability of molecular beam cells. In this study, we conducted a systematic investigation of the thickness-dependent structural evolution of Cu ultrathin films grown on FeCo(100) by MBE.

II. EXPERIMENTAL

Previous reports have demonstrated that high-quality bcc-$Fe_{0.5}Co_{0.5}$(100) thin films can be grown on MgO(100) substrates by both sputtering [5] and MBE [10]. Based on this, we employed FeCo films on MgO(100) as the underlying template for Cu growth. Cu/FeCo(100)/MgO(100) thin films were fabricated by MBE in a UHV chamber with a base pressure of 5×10^{-8} Pa [Figure 1(a)]. To examine thickness-dependent structural behavior, five samples with Cu thicknesses of 1, 3, 4, 5, and 30 nm were prepared. MgO(100) substrates (Crystal Base, 10 mm × 10 mm × 0.5 mm) were annealed at 500 °C for 10 h to obtain clean surfaces. FeCo layers thicker than 15 nm were deposited by electron-beam (EB) evaporation at a substrate temperature of 300 °C with a deposition rate of 0.17 Å min^{-1}. Subsequently, Cu layers were deposited by EB evaporation at room temperature with a deposition rate of 1.3 Å min^{-1}. Deposition rates and film thicknesses were calibrated by a quartz crystal microbalance. The evaporation sources were a high-purity $Fe_{0.5}Co_{0.5}$ rod (TOSHIMA Manufacturing, 2 mm × 2 mm × 20 mm, 4N) and a Cu wire (Nilaco, 0.25 mm in diameter, 5N).

In-situ surface crystallinity was evaluated immediately after sample preparation by low-energy electron diffraction (LEED: OCI BDL600) with the ViPErLEED system [11–13].

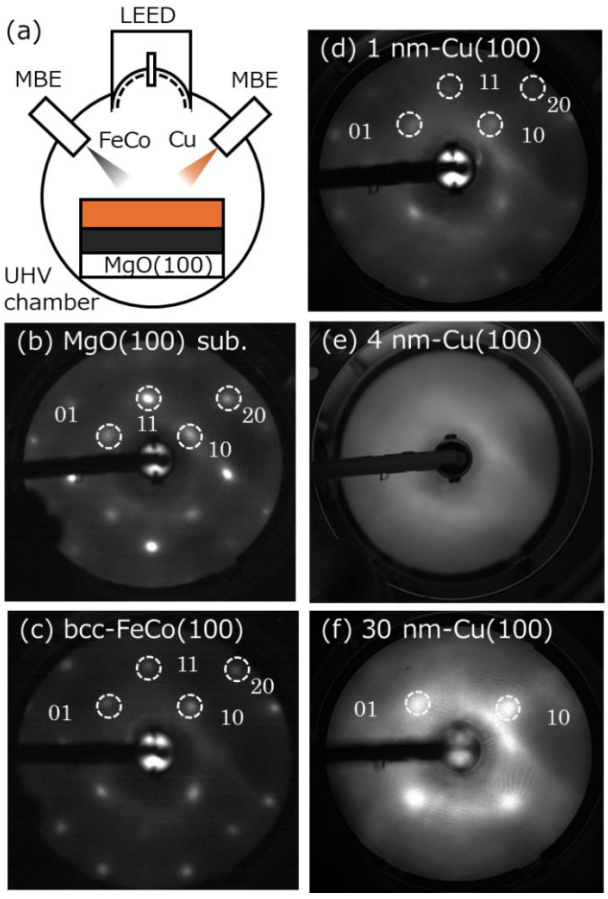


Figure 1: (a) Schematic of sample preparation. (b–f) LEED patterns of each surface at an incident electron energy of 210 eV.

The *R*-factors, which describes the agreement between two LEED-*I*(*V*) spectra, were calculated using Pendry's method [14]. To prevent oxidation during subsequent *ex-situ* measurements, a 1 nm-thick Al capping layer was deposited on the 1, 3, 4, and 5 nm-Cu samples. *Ex-situ* structural characterization was performed using X-ray diffraction (XRD: Rigaku SmartLab) with Cu Kα radiation (45 kV, 200 mA) for all samples. Following XRD measurements, transmission electron microscopy (TEM: FEI Titan G2 80-200) was carried out on the 4 nm-Cu sample. The accelerating voltage was 200 kV. Cross-sectional TEM specimens were prepared using the lift-out technique with a dual-beam focused ion-beam/scanning electron microscope (FIB/SEM: FEI Helios G4). Prior to the specimen preparation, a Pt protection layer was deposited on the surface.

III. RESULTS AND DISCUSSIONS

Figure 1(b, f) shows the LEED images of the samples. Well-defined 1 × 1 diffraction patterns were observed from the bare MgO(100) substrate surface [Figure 1(b)] and from the bcc-FeCo(100) film surface [Figure 1(c)], confirming the formation of clean surfaces. A similarly sharp diffraction pattern was also obtained for the 1 nm-Cu ultrathin film [Figure 1(d)], identical to that of the bcc-FeCo(100) surface [Figure 1(c)]. When the 1 nm-Cu ultrathin film adopts a bcc-Cu(100) structure templated by the underlying bcc-FeCo(100), as reported in previous studies on sputtered films, the diffraction patterns of FeCo(100) and Cu(100) become indistinguishable. In contrast, no diffraction spots were visible for the 3, 4, and 5 nm-Cu films, indicating a loss of structural order at the surface in this intermediate thickness regime. For the 30 nm-Cu film surface [Figure 1(f)], diffraction spots reappeared, signifying the recovery of structural order at the surface. At the same time, the high background intensity suggests the presence of numerous surface defects and steps. Notably, the appearance of the diffraction spots in the 30 nm-Cu film [Figure 1(f)] differs significantly from those of the 1 nm-Cu film [Figure 1(d)].

To further clarify the difference between the LEED diffraction spots of the 1 and 30 nm-Cu films, we measured the *I*(*V*) spectra of the diffraction spots. Figure 2 shows the LEED-*I*(*V*) spectra of the 01 spots from Figure 1(c, d, f), indexed on the basis of previous reports. The *I*(*V*) spectra from all comparable LEED spots, which illustrated in Figure S1 in Supplementary Material, of 1 nm-Cu(100) and FeCo(100) matched well (*R*-factor = 0.19), indicating that the Cu layer inherits the FeCo structure.

The *I*(*V*) spectra from all comparable LEED spots (Figure S1) of 30 nm-Cu(100) deviated strongly from those of 1 nm-Cu(100) (*R*-factor ≧ 0.95), highlighting a thickness-driven structural change. These results indicate that Cu initially adopts a bcc structure templated by the FeCo underlayer, undergoes surface disorder at intermediate thicknesses, then transforms into a different structure at larger thicknesses.

To further clarify this thickness-driven structural evolution in the Cu(100)/FeCo(100) structure, out-of-plane XRD meas-

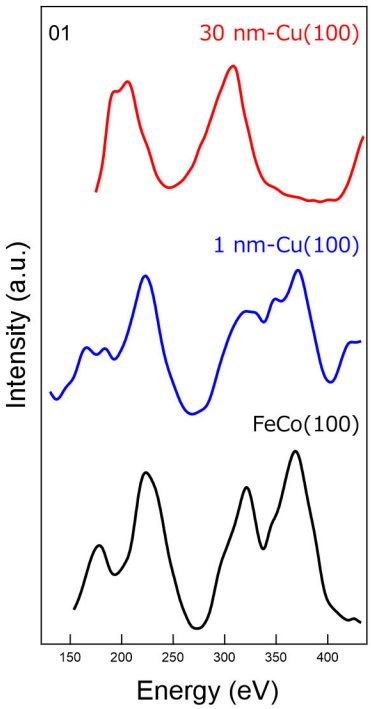


Figure 2: LEED-$I(V)$ spectra from 01 spots, averaged over the four symmetry-equivalent spots for FeCo(100), 1 nm-Cu(100), and 30 nm-Cu(100).

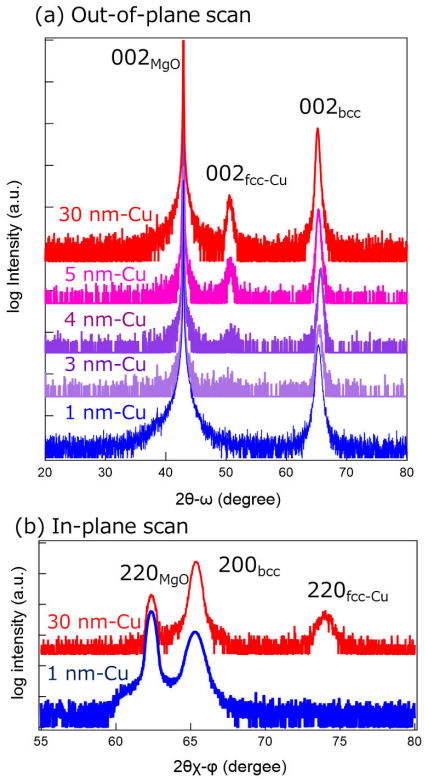


Figure 3: XRD results. (a) Thickness dependence of out-of-plane scan. Each spectrum was normalized with the intensity of 002_{MgO} peaks. (b) In-plane scan.

urements were performed [Figure 3(a)]. A 002_{bcc} diffraction peak originating from the bcc-FeCo layer was observed in all samples. For the 30 nm-Cu film, an additional $002_{fcc\text{-}Cu}$ peak appeared, confirming a transformation into the fcc phase with increasing Cu thickness. Notably, a weak $002_{fcc\text{-}Cu}$ peak was already present at 3 nm, earlier than the 4–5 nm reported for sputtered Cu/TiN(001) films [9], suggesting that the differences in growth method and wettability play a role. Figure 3(b) presents the results of in-plane XRD measurements. In-plane scans of the 30 nm-Cu sample revealed 220_{MgO}, 200_{bcc}, and $220_{fcc\text{-}Cu}$ peaks, establishing the in-plane epitaxial relationship of MgO[110] || FeCo[100] || fcc-Cu[110]. In contrast, the 1 nm-Cu sample exhibited only 220_{MgO} and 200_{bcc} peaks, with no detectable fcc-related peaks.

To examine the structure of the Cu layer in the intermediate thickness regime where LEED spots were not observed, cross-sectional high-angle annular dark-field scanning TEM (HAADF-STEM) and energy-dispersive X-ray spectroscopy (EDS) analysis were performed on the 4 nm-Cu sample [Figure 4(a)]. Variations in contrast within the Cu layer indicated nanoscale steps or island-like structures. EDS mapping further revealed only minor interdiffusion at the Cu/FeCo interface.

The high-magnification image [Figure 4(b)] shows the atomic arrangements of each layer, with the electron beam incident along the bcc[1$\bar{1}$0] direction. The arrangement of atomic columns clearly differs between the FeCo and Cu layers. The FeCo columns exhibited a rectangular periodicity corresponding to bcc[110], whereas the Cu exhibited a square periodicity, which corresponds to fcc[001]. The measured interplanar spacings were 2.0 Å for $(110)_{bcc\text{-}FeCo}$, 1.3 Å for $(001)_{bcc\text{-}FeCo}$, and 1.8 Å for both $(100)_{Cu}$ and $(001)_{Cu}$, as indicated in Figure 4(b). These values are consistent with the calculated spacings from the lattice constants of bcc-FeCo (a = 2.86 Å) and fcc-Cu (a = 3.61 Å) [5, 7]. Together with the presence of the $002_{fcc\text{-}Cu}$ peak in the XRD profile [Figure 3(a)], these findings confirm that the Cu layer is oriented as fcc-Cu[001]. It has been reported that both bcc and fcc phases coexist within the Cu layer in FeCo/4 nm-Cu/FeCo multilayer structures fabricated by sputtering [7]. In contrast, the Cu layer was uniformly in the fcc phase and no bcc phase was detected in our MBE-grown 4 nm-Cu/FeCo sample. This difference is likely attributable not only to the growth method but also to the fact that, in the previous study, both upper and lower interfaces serve as bcc templates, which influences structural stability.

Furthermore, dislocations were observed at the Cu/FeCo interface, including regions where extra half planes of atoms were inserted as marked in Figure 4(b). However, these dislocations were not strictly periodic, instead, irregularly distributed segments were also identified. This indicates that, in addition to lattice mismatch, preexisting defects and roughness at the FeCo surface likely contribute to their formation.

Regarding the surface, while the lattice in the Cu film was clearly observed in the TEM image, no diffraction spots were visible in the LEED image of the 4 nm-Cu sample [Figure 1(e)]. This implies that surface flatness is not well main-

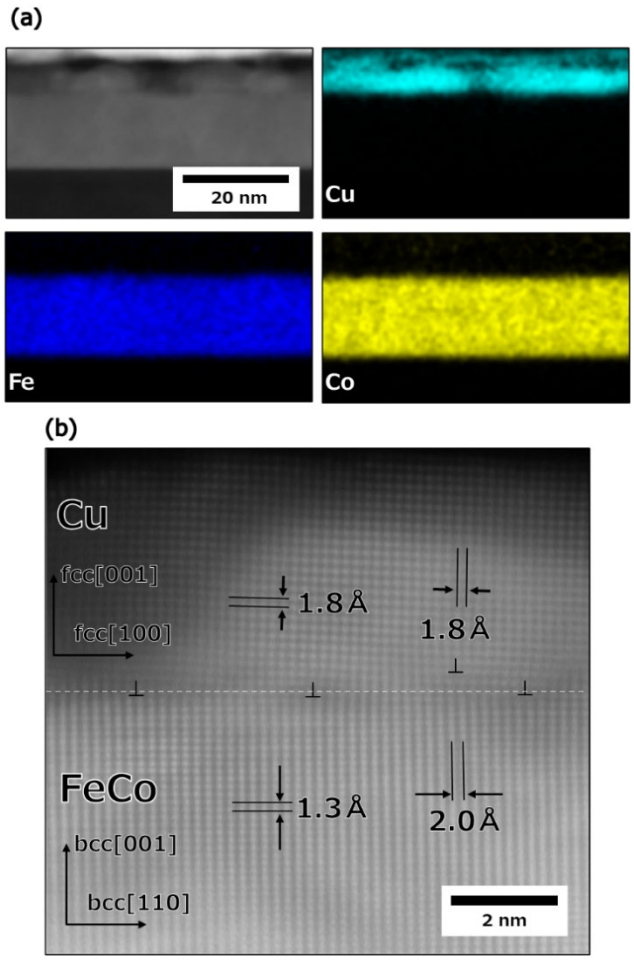


Figure 4: Cross-sectional HAADF-STEM images of 4 nm-Cu, along the $[110]_{bcc\text{-}FeCo}$ direction. (a) Low-magnification image and its EDS elemental mapping. (b) High-magnification image. The ⊥-shape markers indicate the positions of dislocations.

tained at the intermediate thickness regime, as also confirmed in Figure S2 in Supplementary Material. The surface flatness recovered as the film thickness increases. Such a behavior has also been reported for sputter-deposited films [9].

In contrast, for the 1 nm-Cu sample, the presence of sharp 1 × 1 LEED spots [Figure 1(d)] indicates that the surface is well ordered in the ultrathin thickness regime. Furthermore, previous studies have reported that Cu grows in a layer-by-layer on both Fe(100) and Co(100) substrates in this thickness range [15–17]. The surface energy of Cu is lower than that of either Fe or Co. This suggests that, in the initial stages of Cu growth on FeCo(100), the Cu layer covers the entire surface of FeCo. In addition, the low *R*-factor obtained between the *I*(*V*) curves of 1 nm-Cu(100) and FeCo(100) indicates that, these two surfaces share the same underlying structure. These results confirm that the 1 nm-Cu layer is non-amorphous and retains a bcc structure inherited from the FeCo substrate.

In GMR devices, the magnetoresistance ratio is mainly governed by spin-dependent scattering at the interfaces of nonmagnetic/ferromagnetic layers [18]. This scattering is highly sensitive to the atomic arrangement and crystallinity of each layer, and the emergence of fcc Cu has been reported to reduce magnetoresistance ratios [7]. Our results suggest that MBE-grown films are well suited if the thickness of the nonmagnetic Cu layer is around 1 nm, where the bcc structure is preserved.

Collectively, these results provide a comprehensive picture of the growth behavior of Cu ultrathin films on FeCo(100). At the initial stage (1 nm), the Cu layer adopts a bcc structure templated by the FeCo substrate, where a sharp 1 × 1 LEED pattern confirms the formation of an ordered surface. Once the Cu thickness exceeds ~3 nm, the film transforms into the fcc phase, accompanied by surface roughness and interfacial dislocations at the Cu/FeCo interface, while surface flatness recovers at larger thicknesses (≥30 nm). The crystallographic relationship above the intermediate regime (≥4 nm) is established as MgO[110] || FeCo[100] || fcc-Cu[110]. Although MBE-grown films undergo the bcc-to-fcc transition at smaller thicknesses than their sputter-deposited counterparts, MBE uniquely provides clean and well-ordered surfaces in the ultrathin regime (<1 nm), enabling advanced *in-situ* surface-sensitive characterization.

IV. CONCLUSIONS

In this study, Cu/FeCo(100) thin films were successfully grown by MBE, and their thickness-dependent structural evolution was systematically investigated. Ultrathin Cu layers initially exhibited a metastable bcc structure inherited from the structure of the FeCo template. As the Cu thickness increased to several nanometers, the Cu layer transformed into a stable fcc structure. The surface structural order was transiently disrupted at intermediate film thicknesses. Our findings clarify the growth behavior of Cu/FeCo(100), and demonstrate that MBE-grown ultrathin films, though less stable than their sputter-deposited counterparts, uniquely provide atomically clean surfaces in the ultrathin regime, thereby enabling advanced *in-situ* surface-sensitive characterization.

Acknowledgments

The authors thank Mr. Fumiya Arai for technical supports, and also thank Dr. Shunsuke Tsuda and Dr. Fumio Komori for discussions. This work was particularly supported by JST CREST, Japan (Grant Numbers: JPMJCR21O1, JPMJCR21O4), JST PRESTO, Japan (Grant Numbers: JPMJPR17NB, JPMJPR20T7), JSPS/MEXT KAKENHI, Japan (Grant Numbers: 25K01628, 24K01243, 24K01352, 21H01638, 21H04696), the Innovative Science and Technology Initiative for Security, ATLA, Japan (Grant Number: JPJ004596), and Advanced Research Infrastructure for Materials and Nanotechnology in Japan (ARIM), of MEXT (Grant Numbers: JPMXP1225NM5366, JPMXP1224NM5290), and JST SPRING (Grant Number: JPMJSP2151). This research was funded in part by the Austrian Science Fund (FWF) under doi:10.55776/F8100, Taming Complexity in Materials Modeling (TACO).

Appendix

The $I(V)$ spectra from all comparable LEED spots and an additional HAADF-STEM image are available in Supplementary Material at https://doi.org/10.1380/ejssnt.2026-004.

References

[1] N. Kaiser, Appl. Opt. **41**, 3053 (2002).
[2] H. Li, D. Tian, J. Quinn, Y. S. Li, F. Jona, and P. M. Marcus, Phys. Rev. B **43**, 6342 (1991).
[3] Q. Guo and G. B. Thompson, Acta Mater. **148**, 63 (2018).
[4] Z. Q. Wang, S. H. Lu, Y. S. Li, F. Jona, and P. M. Marcus, Phys. Rev. B **35**, 9322(R) (1987).
[5] K. B. Fathoni, Y. Sakuraba, T. Sasaki, Y. Muira, J. W. Jung, T. Nakatani, and K. Hono, APL Mater. **7**, 111106 (2019).
[6] D. Taparia, K. B. Fathoni, P. D. Kulkarni, A. Srinvasan, P. Alagarsamy, Y. Sakuraba, T. Nakatani, and K. Hono, J. Magn. Magn. Mater. **538**, 168321 (2021).
[7] K. B. Fathoni, Z. Li, T. Nakatani, Y. Sakuraba, T. Sasaki, and K. Hono, J. Magn. Magn. Mater. **551**, 169154 (2022).
[8] H. Nakayama, B. Xu, S. Iwamoto, K. Yamamoto, R. Iguchi, A. Miura, T. Hirai, Y. Miura, Y. Sakuraba, J. Shiomi, and K. Uchida, Appl. Phys. Lett. **118**, 042409 (2021).
[9] R. Namakian, B. R. Novak, X. Zhang, W. J. Meng, and D. Moldovan, Appl. Surf. Sci. **570**, 151013 (2021).
[10] K. Shikada, M. Ohtake, F. Kirino, and M. Futamoto, J. Appl. Phys. **105**, 07C303 (2009).
[11] F. Kraushofer, A. M. Imre, G. Franceschi, T. Kißlinger, E. Rheinfrank, M. Schmid, U. Diebold, L. Hammer, and M. Riva, Phys. Rev. Res. **7**, 013005 (2025).
[12] M. Schmid, F. Kraushofer, A. M. Imre, T. Kißlinger, L. Hammer, U. Diebold, and M. Riva, Phys. Rev. Res. **7**, 013006 (2025).
[13] F. Dörr, M. Schmid, L. Hammer, U. Diebold, and M. Riva, in preparation.
[14] J. B. Pendry, J. Phys. C **13**, 937 (1980).
[15] B. Heinrich, Z. Celinski, J. F. Cochran, W. B. Muir, J. Rudd, Q. M. Zhong, A. S. Arrott, K. Myrtle, and J. Kirschner, Phys. Rev. Lett. **64**, 673 (1990).
[16] P. LeClair, H. J. M. Swagten, J. T. Kohlhepp, R. J. M. van de Veerdonk, and W. J. M. de Jonge, Phys. Rev. Lett. **84**, 2933 (2000).
[17] D. Kerkmann, D. Pescia, J. W. Krewer, and E. Vescovo, Z. Phys. B **85**, 311 (1991).
[18] P. Barla, V. K. Joshi, and S. Bhat, J. Comput. Electron. **20**, 805 (2021).

All articles published on e-J. Surf. Sci. Nanotechnol. are licensed under the Creative Commons Attribution 4.0 International (CC BY 4.0). You are free to copy and redistribute articles in any medium or format and also free to remix, transform, and build upon articles for any purpose (including a commercial use) as long as you give appropriate credit to the original source and provide a link to the Creative Commons (CC) license. If you modify the material, you must indicate changes in a proper way.

Copyright: ©2026 The author(s)
Published by The Japan Society of Vacuum and Surface Science